Title

Power optimization of wireless media systems with space-time block codes

Permalink

https://escholarship.org/uc/item/84x507gj

Journal

IEEE Transactions on Image Processing, 13(7)

ISSN

1057-7149

Authors

Yousefi'zadeh, H
Jafarkhani, H
Moshfeghi, M

Publication Date

2004-07-01

Peer reviewed

Power Optimization of Wireless Media Systems With Space-Time Block Codes

Homayoun Yousefi'zadeh, *Member, IEEE*, Hamid Jafarkhani, *Senior Member, IEEE*, and Mehran Moshfeghi

Abstract—We present analytical and numerical solutions to the problem of power control in wireless media systems with multiple antennas. We formulate a set of optimization problems aimed at minimizing total power consumption of wireless media systems subject to a given level of QoS and an available bit rate. Our formulation takes into consideration the power consumption related to source coding, channel coding, and transmission of multiple-transmit antennas. In our study, we consider Gauss–Markov and video source models, Rayleigh fading channels along with the Bernoulli/Gilbert–Elliott loss models, and space–time block codes.

Index Terms—Bernoulli and Gilbert–Elliott loss models, multiple antenna systems, power optimization, QoS, source/channel coding, space-time block codes, wireless media systems.

INTRODUCTION

WIRELESS devices are proliferating at a rapid rate. Broadband wireless coverage is extensive in many areas and there has been an exponential growth in the processing power of embedded processors. The emergence of new wireless standards is expected to expedite the delivery of the next generation portable multimedia services such as disaster relief, surveillance, and videoconferencing. More frequent and longer use of portable multimedia services is naturally equivalent to higher power consumption of mobile devices. Added to this the fact that the battery life is growing far more slowly than the processing power in handheld devices, the power consumption of such devices is required to be kept to a minimum level in order to extend the lifetime of their limited power resources. On the contrary, providing the desired level of quality of service (QoS) in the presence of the fading effects of multipath wireless channels necessitates higher consumption of power in mobile devices. Power optimization is, therefore, very important because it extends the lifetime of batteries.

Multiple antenna systems substantially reduce the effect of multipath fading in wireless channels through antenna diversity. Antenna diversity has been adopted in WCDMA and CDMA2000 standards. It is also being considered in many current wireless standard efforts. A large percentage of next generation mobile devices such as cellular phones, global positioning systems (GPS), personal digital assistants (PDA), and laptops will, therefore, employ multiple antennas. Hence, it is essential to consider systems using multiple antennas in the

study of wireless media systems. In what follows, we provide a review of the literature.

In an early work, Lan *et al.* [12] solved an energy optimization problem subject to QoS constraints for transmitting images across the wireless backbone. However, they did not consider the time-varying characteristics of the wireless channel in the analysis of channel coding and transmission. Goel *et al.* [7] solved another image transmission energy optimization problem subject to distortion and rate constraints. While they appropriately considered hardware specific impacts in their work, their analysis lacked a consideration of channel coding and transmission with respect to the time-varying characteristics of the wireless channel. Having a [8] considered energy efficiency in channel coding techniques for wireless systems without considering the energy of source coding and transmission. Stuhlmuller *et al.* [16] derived a rate-distortion model for an H.263 compliant coder based on simulation data. Their model could also be used for other codecs that rely on hybrid motion compensation. Appadwedula *et al.* [4] formulated and solved an energy optimization problem subject to statistical distortion and rate constraints for transmitting images over wireless channels. The authors considered transmission, source, and channel-coding components in the formulation of the problem. Ji *et al.* [11] proposed a generic motion estimation technique that could well fit into H.263 or MPEG-2 source coding standards. They used an unequal error protection (UEP) technique based on the Bernoulli loss model in conjunction with Reed–Solomon (RS) channel coding. Focusing on an uplink mobile-to-base scenario, Lu *et al.* [13] solved a similar power optimization problem subject to the end-to-end distortion of [16] relying on H.263 source coding and RS channel coding in conjunction with the Gilbert loss model. A preliminary version of this work [10] analytically solved a similar problem under the Bernoulli loss model with an additional rate constraint while deploying space-time block codes. We point out that although the use of multiple antennas cannot be ignored as the result of adoption in the new wireless standards, none of the literature articles cited above have considered deploying multiple antennas in wireless systems. Further, none of the literature articles has provided an analysis of complexity when solving their formulated optimization problem. Considering the real-time nature of the problem, we argue that providing a low complexity solution to a power optimization problem is important.

An outline of the remaining parts of the paper follows. In Section II, we express our motivation and contributions. In Section III, we provide an analysis of the transmission and the channel coding components of the underlying wireless system.

In this section, we express the symbol error rate as a function of the average received signal-to-noise ratio and the loss model. In Section IV, we provide an analysis of the source coding and distortion for the underlying wireless system. Starting from a simple Gauss–Markov source model, we generalize our analysis to a video source and obtain associated overall distortions for each case. In Section V, we formulate and solve our power optimization problem subject to distortion and rate constraints. In Section VI, we numerically validate our results. Finally, Section VII includes a discussion of concluding remarks and future work.

I. MOTIVATION AND CONTRIBUTIONS

The theme representing the goal of this paper is to study the end-to-end problem of multimedia transmission over a wireless channel with multiple-transmit/receive antennas. We address the tradeoff between the power consumption and the quality of service in wireless media systems. Our goal is to minimize the overall power consumption for a given quality of service and a given bit rate. Fig. 1 illustrates the general model of a communication system used to transmit multimedia content across a wireless backbone. We note that the model may use one or more transmit and/or receive antennas.

Optimizing power for transmitting multimedia content from a mobile host requires addressing the consumption tradeoff among different components of the underlying communication system. The power consumed in a transmitting mobile device is for the most part associated with source coding, channel coding, and transmission. The power of source coding and channel coding is typically a function of the underlying algorithms. The transmission power depends on the overall transmission bit rate and the symbol transmission energy. Intuitively, a higher QoS and a higher bit rate result in more power consumption. In this paper, the received signal distortion is used as the metric of measuring QoS. Signal distortion has two components. The first component is the distortion caused by source coding compression and decompression. The second component is the distortion caused by having unrecoverable channel coding errors. The available bit rate is divided between the source coding information and the channel coding redundancy assigned for error recovery.

We independently describe each of the terms involved in the formulation of our power optimization problem followed by the formulation of the problem itself. We will then focus on providing efficient methods of solving our problem and validating our results.

The main contributions of this paper are in the following areas. First, we propose the use of multiple antenna systems along with space-time block codes in addition to traditional single antenna systems. Second, we consider three different channel loss models, namely Bernoulli, Gilbert, and Gilbert–Elliott models, to properly capture the loss behavior of different transmission channels. While we rely on closed-form expressions of the loss model in the first two cases, we use a recursive expression to describe the behavior of the last loss model. Third, relying on the analysis of multiple antenna systems along with various channel loss models, we formulate
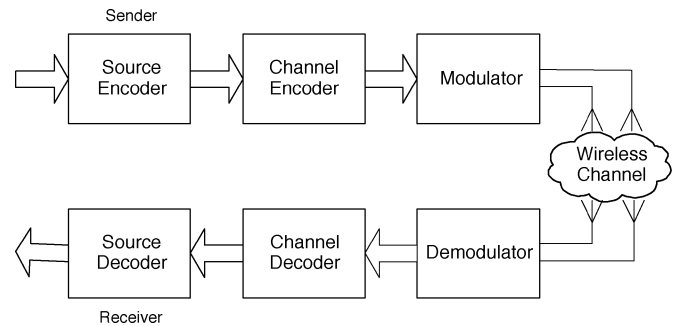

Fig. 1. Illustration of the multiple antenna communication system.

a set of power optimization problems aimed at minimizing the combined power of source coding, channel coding, and transmission while considering rate and distortion constraints. We provide analytical solutions to the optimization problems utilizing Bernoulli and Gilbert loss models and a numerical solution to the optimization problem using the Gilbert–Elliott loss model.

II. TRANSMISSION AND CHANNEL CODING ANALYSIS

We start our discussion by providing an analysis of the transmission system and the wireless fading channel.

A. Transmission and Fading Channel Analysis

First, we focus on the analysis of the wireless fading channel. We rely on the so-called Rayleigh model with a fading factor α to describe the wireless channel. We note that the output signal of such a channel S_o can be related to its input signal S_i as

$$S_o = \alpha S_i + N \tag{1}$$

where N indicates the noise signal. Further, we recall that for a multipath slow fading Rayleigh wireless channel, the per bit average received signal-to-noise ratio $\overline{\text{SNR}}$ is expressed as

$$\overline{\text{SNR}} = \mathcal{E}\left[|\alpha|^2\right] \frac{E_{\text{sym}}}{N_0} \tag{2}$$

where $\mathcal{E}$ denotes the expectation operator, $|\alpha|$ has a Rayleigh distribution, E_{sym} is the transmission energy per symbol interval, and N_0 is the one-sided spectral density of the white Gaussian noise. We note that while the transmission energy per symbol interval is the same as the transmission symbol energy in the case of a one transmit antenna system, it is split in half between the two symbols transmitted at each symbol interval in the case of a double-transmit antenna system. Nevertheless, we note that (2) can be properly applied to the cases of both single and double-transmit antenna systems. In our discussion below, we consider the fact that the asymptotic behavior of the symbol error rate for large values of $\overline{\text{SNR}}$ can be described as $e_{\text{sym}} \simeq G_c \overline{\text{SNR}}^{-G_d}$ where G_c and G_d represent coding gain and diversity gain, respectively. Next, assuming a slow fading Rayleigh channel and utilization of the L-PSK modulation scheme, we calculate closed-form expressions describing the symbol error rate of a multiple-transmit multiple-receive antenna system. Starting from [15, eq. (9.15)] of the work of Simon et al. with the choice of $g_{\text{PSK}} = \overline{\text{SNR}} \sin^2(\pi/L)$ and

$M_1(x, \overline{\text{SNR}}) = \cdots = M_L(x, \overline{\text{SNR}}) = (1 - x\overline{\text{SNR}})^{-1}$, the symbol error rate of a single transmit M receive antenna system using maximum ratio combining (MRC) can be calculated as

$$e_{\text{sym}} = \frac{1}{\pi} \int_0^{\frac{(L-1)\pi}{L}} \left[M\left(-\frac{\overline{\text{SNR}}\sin^2\left(\frac{\pi}{L}\right)}{\sin^2\phi}, \overline{\text{SNR}} \right) \right]^L d\phi$$

$$= \frac{1}{\pi} \int_0^{\frac{(L-1)\pi}{L}} \left[\frac{\sin^2\phi}{\sin^2\phi + \overline{\text{SNR}}\sin^2\left(\frac{\pi}{L}\right)} \right]^L d\phi. \quad (3)$$

We note that (3) holds under the assumption that the fading is identically distributed with the same fading parameter and the same $\overline{\text{SNR}}$ for all of the L channels associated with the transmit and individual receive antennas. Further, we note that diversity gain is in the order of the product of the transmit and the receive antennas. Hence, a single transmit M receive antenna system has a diversity gain of order M. The closed-form solution to the integral of (3) is expressed as

$$e_{\text{sym}} = \frac{L-1}{L} - \frac{1}{\pi}\sqrt{\frac{\vartheta}{1+\vartheta}}$$

$$\times \left\{ \left(\frac{\pi}{2} + \tan^{-1}\xi\right) \sum_{j=0}^{M-1} \binom{2j}{j} \frac{1}{[4(1+\vartheta)]^j} + \sin(\tan^{-1}\xi) \right.$$

$$\left. \times \sum_{j=1}^{M-1}\sum_{i=1}^{j} \frac{\tau_{ij}}{(1+\vartheta)^j} \left[\cos(\tan^{-1}\xi)\right]^{2(j-i)+1} \right\} \quad (4)$$

where $\vartheta = \overline{\text{SNR}}\sin^2(\pi/L)$, $\xi = \sqrt{\vartheta/(1+\vartheta)}\cot(\pi/L)$ and $\tau_{ij} = (\binom{2j}{j}/(\binom{2(j-i)}{j-i}4^i[2(j-i)+1]))$. Noting that the number of bits per symbol m is related to the number of signal points in the constellation L as $m = \log_2 L$, the result of (4) for a single-transmit single-receive antenna system where $M = 1$ and QPSK modulation where $m = 2$ and $L = 4$ is expressed as

$$e_{\text{sym}} = \frac{3}{4}\left\{ 1 - \frac{4}{3\pi}\sqrt{\frac{\overline{\text{SNR}}}{2+\overline{\text{SNR}}}} \right.$$

$$\left. \times \left[\frac{\pi}{2} + \arctan\sqrt{\frac{\overline{\text{SNR}}}{2+\overline{\text{SNR}}}}\right] \right\}. \quad (5)$$

Similarly, the result of (4) for a single-transmit double-receive antenna system where $M = 2$ and QPSK modulation is expressed as

$$e_{\text{sym}} = \frac{3}{4} - \frac{\zeta}{\pi}\left\{ \left(\frac{\pi}{2} + \tan^{-1}\zeta\right)\left(1 + \frac{1}{2+\overline{\text{SNR}}}\right) \right.$$

$$\left. + \sin(2\tan^{-1}\zeta)\left(\frac{1}{2(2+\overline{\text{SNR}})}\right) \right\} \quad (6)$$

where $\zeta = [(\overline{\text{SNR}})/(2+\overline{\text{SNR}})]^{1/2}$. We observe that the symbol error rate of a single-transmit double-receive antenna system is improved compared to that of a single-transmit single-receive antenna system due to the receive diversity gain. Next, we investigate the symbol error rate for multiple-transmit antenna systems. We consider the space-time block codes (STBCs) of [1] and [19] as they have been adopted by WCDMA and

CDMA2000 wireless standards. We note that STBCs achieve the maximum diversity gain. Recalling that the diversity gain is in the order of the product of the transmit and the receive antennas, we note that a double-transmit single-receive antenna system achieves the same diversity gain as a single-transmit double-receive antenna system. Under the assumption of a fixed total amount of power available at the transmitter, in each symbol interval the power is split equally between the two antennas for a double-transmit single-receive antenna system. On the contrary, in the case of a single-transmit double-receive antenna system, only one symbol is transmitted in each symbol interval and the total energy is allocated to it. Therefore, taking into consideration the results of [18], the efficiency of the former scheme suffers a 3 dB loss with respect to that of the latter scheme from the standpoint of the coding gain. Hence, by replacing $\overline{\text{SNR}}$ with $(\overline{\text{SNR}}/2)$ in (6), one can obtain the symbol error rate of a double-transmit single-receive antenna system utilizing QPSK modulation as

$$e_{\text{sym}} = \frac{3}{4} - \frac{\zeta}{\pi}\left\{ \left(\frac{\pi}{2} + \tan^{-1}\zeta\right)\left(1 + \frac{2}{4+\overline{\text{SNR}}}\right) \right.$$

$$\left. + \sin(2\tan^{-1}\zeta)\left(\frac{1}{4+\overline{\text{SNR}}}\right) \right\} \quad (7)$$

where $\zeta = [(\overline{\text{SNR}})/(4+\overline{\text{SNR}})]^{1/2}$. Under the same line of reasoning, one can obtain the symbol error rate of a double-transmit double-receive antenna system. Replacing $\overline{\text{SNR}}$ with $(\overline{\text{SNR}}/2)$ in QPSK results from a single-transmit quad receive antenna system yields

$$e_{\text{sym}} = \frac{3}{4} - \frac{1}{\pi}\sqrt{\frac{\overline{\text{SNR}}}{4+\overline{\text{SNR}}}}$$

$$\times \left\{ \left(\frac{\pi}{2} + \tan^{-1}\zeta\right) \sum_{j=0}^{3} \binom{2j}{j} \frac{1}{[4+\overline{\text{SNR}}]^j} + \sin(\tan^{-1}\zeta) \right.$$

$$\left. \times \sum_{j=1}^{3}\sum_{i=1}^{j} \frac{4\tau_{ij}}{(4+\overline{\text{SNR}})^j} \left[\cos(\tan^{-1}\zeta)\right]^{2(j-i)+1} \right\} \quad (8)$$

where $\zeta = [(\overline{\text{SNR}})/(4+\overline{\text{SNR}})]^{1/2}$ and τ_{ij} is the element located at row i and column j of matrix τ defined as follows:

$$\tau = \begin{bmatrix} 0.5000 & 0.2500 & 0.1667 \\ 0 & 0.3750 & 0.2083 \\ 0 & 0 & 0.3125 \end{bmatrix}.$$

We also note that various BPSK results can be obtained similarly by setting $L = 2$ in (4). We finish this section by noting that the per symbol average signal-to-noise ratio $\overline{\text{SNR}}_{\text{sym}}$ is related to the per bit average signal-to-noise ratio $\overline{\text{SNR}}$ as $\overline{\text{SNR}}_{\text{sym}} = m\overline{\text{SNR}}$. Consequently, for the choice of normalization factors $m = (N_0/\mathcal{E}[|\alpha|^2])$, the relationship $\overline{\text{SNR}}_{\text{sym}} = E_{\text{sym}}$ holds.

B. Loss and Channel Coder Analysis

Having specified the symbol error rate based on the channel characteristics, we propose utilizing a Reed–Solomon channel coder $\text{RS}(n,k)$ that converts k information symbols into an n-symbol block as the result of appending $(n - k)$ parity symbols. Assuming R_s and R_c respectively denote source

and channel coding bit rates, we note that utilizing such a channel coding scheme introduces a channel code rate $r = (k/n) = R_s/(R_s + R_c)$. The scheme also allows for correcting $t_c = \lfloor (n - k)/2 \rfloor$ symbol errors. In order to calculate the error rate of a block utilizing an $RS(n, k)$ coder, we consider the single-state Bernoulli, the two-state Gilbert [6], and the two-state Gilbert–Elliott [3] error models. We note that while the first model represents a memoryless channel, the other two represent channels with memory. It is also important to note that the second model is a special case of the third model.

The single state Bernoulli model is the simplest model describing symbol loss in a memoryless channel. In the Bernoulli model, one assumes that the probabilities of loss among different symbols are temporally independent. Noting the fact that losing more than t_c symbols from n transmitted symbols results in a block loss, the probability of block loss, also known as the residual symbol error rate, for the Bernoulli model is given by

$$\Psi(n, t_c) = \sum_{i=t_c+1}^{n} \binom{n}{i} e_{\mathrm{sym}}^i (1 - e_{\mathrm{sym}})^{(n-i)} \quad (9)$$

where e_{sym} is the symbol error rate.

As pointed out in many research articles, a multipath fading wireless channel typically undergoes burst loss representing temporally correlated loss. The two-state Gilbert loss model provides an elegant mathematical model to capture the loss behavior of ever-changing channel conditions. In the Gilbert model, symbol loss is described by a two-state Markov chain as described in Fig. 2. The first state G, known as the GOOD state, represents the loss of a symbol with probability $e_G = 0$ or no symbol loss at all, while the other state B, known as the BAD state, represents the loss of a symbol with probability $e_B = 1$. The GOOD state also introduces a probability $P_G = \gamma$ of staying in the GOOD state and a probability $1 - P_G$ of transitioning to the BAD state while the BAD state introduces a probability $P_B = \beta$ of staying in the BAD state and a probability $1 - P_B$ of transitioning to the GOOD state. The parameters γ and β can be typically measured from the observed loss rate and burst length. In [20], we study temporally correlated loss behavior of IP packet networks employing the two-state Gilbert loss model. In that article, we show that for the Gilbert loss model, the closed-form expression for the probability of receiving exactly k symbols from n transmitted symbols is given by

$$P(n, k) = P(n, k, G) + P(n, k, B). \quad (10)$$

The probability of receiving exactly k symbols from n transmitted symbols and winding up in the GOOD state $P(n, k, G)$ is given by

$$P(n, k, G) = \gamma^{2k-n}(1 - \beta)(1 - \gamma)$$
$$\times \left\{ \sum_{i=0}^{n-k-1} \binom{n-k-1}{i} \binom{k}{i+1} \right.$$
$$\left. \times (\beta\gamma)^{n-k-1-i} [(1 - \beta)(1 - \gamma)]^i \right\}$$
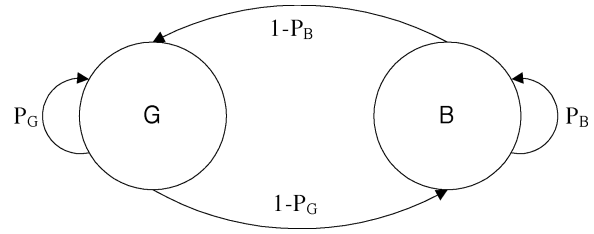$$\times g_{ss} + \gamma^{2k-n-1}(1 - \beta)$$

Fig. 2. Two-state Gilbert loss model with the state transition probabilities $1 - P_G$ and $1 - P_B$ for $P_G = \gamma$ and $P_B = \beta$. The symbol loss probabilities are specified by $e_G = 0$ and $e_B = 1$.

$$\times \left\{ \sum_{i=0}^{n-k} \binom{n-k}{i} \binom{k-1}{i} (\beta\gamma)^{n-k-i} \right.$$
$$\left. \times [(1 - \beta)(1 - \gamma)]^i \right\} b_{ss} \quad (11)$$

for $n \geq k + 1$, steady state probability of the GOOD state $g_{ss} = (1 - \beta)/(2 - \gamma - \beta)$, and steady-state probability of the BAD state $b_{ss} = (1 - \gamma)/(2 - \gamma - \beta)$. Similarly, the probability of receiving exactly k symbols from n transmitted symbols and winding up in the BAD state $P(n, k, B)$ is given by

$$P(n, k, B) = \gamma^{2k-n+1}(1 - \gamma)$$
$$\times \left\{ \sum_{i=0}^{n-k-1} \binom{n-k-1}{i} \binom{k}{i} \right.$$
$$\left. \times (\beta\gamma)^{n-k-1-i} [(1 - \beta)(1 - \gamma)]^i \right\}$$
$$\times g_{ss} + \gamma^{2k-n}(1 - \beta)(1 - \gamma)$$
$$\times \left\{ \sum_{i=0}^{n-k-1} \binom{n-k}{i+1} \binom{k-1}{i} \right.$$
$$\left. \times (\beta\gamma)^{n-k-1-i} [(1 - \beta)(1 - \gamma)]^i \right\} b_{ss}. \quad (12)$$

The initial conditions for (11) and (12) are expressed as follows:

$$P(k, 0, G) = 0$$
$$P(k, k, B) = 0$$
$$P(k, k, G) = \gamma^k g_{ss} + (1 - \beta)\gamma^{(k-1)} b_{ss}$$
$$P(k, 0, B) = (1 - \gamma)\beta^{(k-1)} g_{ss} + \beta^k b_{ss}. \quad (13)$$

While our model is of special interest from the standpoint of providing an analytical lower complexity solution to a power optimization problem such as the one proposed in [13], we take a step further in this study by utilizing the Gilbert–Elliott loss model to best describe the loss behavior of a wireless channel. We note that the two-state Gilbert–Elliott loss model is a generalization of the two-state Gilbert loss model with nontrivial symbol loss error probabilities e_G and e_B, where $e_G \ll e_B$. In [9], we provide effective ways of measuring the parameters of the Gilbert–Elliott loss model. Further, the work of [17] describes how different methods of capturing memory in analog communication channels such as Doppler's shift in Rayleigh fading or Jake's fading model can be related to capturing memory in digital communication channels such as the Gilbert–Elliott model. For the Gilbert–Elliott loss model, the probability of receiving exactly k symbols from n transmitted symbols is still described by (10). However, the recursive

probabilities of receiving exactly k symbols from n transmitted symbols and winding up in the GOOD state and the BAD state are respectively given by

$$
\begin{aligned}
P(n,k,G) = e_G \, [&\gamma P(n-1,k,G) \\
&+(1-\beta)P(n-1,k,B)] + \\
&(1-e_G) \times [\gamma P(n-1,k-1,G) \\
&+(1-\beta)P(n-1,k-1,B)] \quad (14)
\end{aligned}
$$

and

$$
\begin{aligned}
P(n,k,B) = e_B \, [&(1-\gamma)P(n-1,k,G) \\
&+\beta P(n-1,k,B)] + \\
&(1-e_B) \times [(1-\gamma)P(n-1,k-1,G) \\
&+\beta P(n-1,k-1,B)] \quad (15)
\end{aligned}
$$

for $n \geq k > 0$ and the initial conditions

$$
\begin{aligned}
P(0,0,G) &= g_{ss} = \frac{1-\beta}{2-\gamma-\beta} \\
P(0,0,B) &= b_{ss} = \frac{1-\gamma}{2-\gamma-\beta} \\
P(1,0,G) &= e_G \, [\gamma g_{ss} + (1-\beta)b_{ss}] \\
P(1,0,B) &= e_B \, [(1-\gamma)g_{ss} + \beta b_{ss}]. \quad (16)
\end{aligned}
$$

Utilizing (10) along with (14) and (15) for the Gilbert–Elliott model, the probability of a block loss is given by

$$
\Psi(n,t_c) = 1 - \sum_{k=n-t_c}^{n} P(n,k). \quad (17)
$$

It is also important to note that using the two-state Gilbert–Elliott model calls for changing (2) in order to distinguish between the symbol error rates of the GOOD state and the BAD state. Assuming $\mathcal{E}[|\alpha_G|^2]$ denotes the expectation of the square of the envelope in the GOOD state, the average received signal-to-noise ratio of the GOOD state is expressed as

$$
\overline{\mathrm{SNR}}_G = \mathcal{E}\,[|\alpha_G|^2] \, \frac{E_{\mathrm{sym}}}{N_0}. \quad (18)
$$

Similarly, the average received signal-to-noise ratio of the BAD state is expressed as

$$
\overline{\mathrm{SNR}}_B = \mathcal{E}\,[|\alpha_B|^2] \, \frac{E_{\mathrm{sym}}}{N_0} \quad (19)
$$

where $\mathcal{E}[|\alpha_G|^2] \gg \mathcal{E}[|\alpha_B|^2]$ and the other parameters are the same as in (2).

III. SOURCE CODING AND DISTORTION ANALYSIS

In this section, we focus on the source coding and the distortion analysis. In order to validate our model, we first provide an analysis of distortion utilizing a Gauss–Markov source model and then continue with an experimental video source model.

A. Analysis of Distortion Based on the Gauss–Markov Source Model

In this subsection, we provide an analysis of the distortion utilizing the so-called Gauss–Markov model. We note that the analysis of this section is provided as a proof of concept. In the next section, we provide an analysis for a more realistic model using an experimental H.263 video source coding model.

For the source coding analysis of this section, we use a first-order Gauss–Markov source with a variance σ_{gm}^2 and a correlation coefficient ρ. As described in [5], utilizing such a model for a transform coder introduces an operational distortion-rate function in the form of

$$
D_{tc}(R_s) = \xi \sigma_{gm}^2 (1-\rho^2)^{\frac{\eta-1}{\eta}} 2^{-2R_s} \quad (20)
$$

where η is the block length of the transform coder, ξ is a constant depending on the quantizer used for the transform coefficients, and R_s is defined in the previous section. We note that the Gauss–Markov model of (20) is reduced to a pure Gaussian source model by setting $\rho = 0$. Hence, the following discussion is also applied to a pure Gaussian source. For a Gauss–Markov source, any symbol associated with an unrecovered block at the channel coder is best represented by the Gaussian mean. Such a representation results in an average distortion of σ_{gm}^2. Consequently, the overall distortion at the decoder is calculated by taking the average of block recovery and block loss distortions multiplied by their associated probabilities. Assuming a block loss probability of $\Psi(n, t_c)$, the overall distortion D_{total} is calculated as

$$
\begin{aligned}
D_{\mathrm{total}} &= D_s + D_v \\
&= (1 - \Psi(n,t_c)) \, D_{tc} + \Psi(n,t_c)\sigma_{gm}^2. \quad (21)
\end{aligned}
$$

Again, we note that the probability of a block loss can be calculated from (9) and (17) in the case of utilizing the Bernoulli loss model and the Gilbert (or the Gilbert–Elliott) loss model, respectively.

B. Analysis of Distortion Based on an Experimental H.263 Video Source Model

Here, we provide an analysis of distortion utilizing a more realistic H.263 compliant source coder. For the source coding analysis of this section, we rely on the experimental results of Stuhlmuller *et al.* [16]. The experimental distortion model of [16] consists of two components D_s and D_v respectively imposed by the source encoder and the channel noise. The model relies on an INTRA update scheme forcing a macroblock (MB) to be coded in the INTRA-mode after every $T-1$ MBs and resulting in a source encoder distortion of

$$
D_s(\omega, R_s) = \frac{\theta(\omega)}{R_s - R_I(\omega)} + D_I(\omega) \quad (22)
$$

where $\omega = (1/T)$ is the INTRA rate, R_s is the encoding bit rate in kilobits per second (kbps), and D_s is the distortion in terms of the mean square error per source sample. The measurements of [16] also suggest that the distortion-rate parameters θ, R_0, and D_0 depend linearly on the percentage of INTRA coded macro blocks ω, as shown by the following equations:

$$
\begin{aligned}
\theta &= \theta_P + \Delta\theta_P \, \omega \\
R_I &= R_{IP} + \Delta R_{IP} \, \omega \\
D_I &= D_{IP} + \Delta D_{IP} \, \omega. \quad (23)
\end{aligned}
$$

The model parameters θ_P, $\Delta\theta_P$, R_{IP}, ΔR_{IP}, D_{IP}, and ΔD_{IP} characterize the coding of the input video sequence with the given motion-compensated H.263 encoder in baseline mode. It is important to note that the parameters highly depend on the spatial detail and the amount of motion in the sequence.

Reference [16] also proposes that the video coder distortion caused by transmission errors is expressed as

$$D_v(\omega, \Psi) = \sigma_{u0}^2 \Psi(n, t_c) \sum_{t=0}^{T-1} \frac{1 - \omega t}{1 + \lambda t} \tag{24}$$

where leakage λ describes the efficiency of loop filtering to remove the error and σ_{u0}^2 describes the sensitivity of the video decoder to an increase in error rate. In addition, the the probability of a block loss $\Psi(n, t_c)$ can be calculated as described in the previous section. The overall distortion D_{total} at the video decoder is then calculated as

$$D_{\text{total}} = D_s + D_v. \tag{25}$$

IV. POWER OPTIMIZATION

In this section, we focus on power optimization of a mobile device used in a wireless media system with space-time block codes. Recalling that the overall power consumed in a mobile device is associated with source coding, channel coding, and transmission, we first introduce individual terms expressing the consumed power of different components. We then proceed with the formulation of the power optimization problem and the solution to it.

A. Power-Optimization Formulation

The first power consumption component of the underlying wireless system is the source encoder. We consider the power consumption of the source encoder in the case of utilizing both the Gauss–Markov source of Section IV-A and the video source of Section IV-B.

We start by considering the power consumption of the Gauss–Markov source encoder of Section IV-A. Considering the fact that the encoder rate is the dominant factor of the power consumption of a Gauss–Markov source encoder, we express the power consumption of such a source encoder as a linear function of the encoder rate, i.e.

$$P_s(R_s) = \epsilon_s(a_{ls} + c_{ls} R_s) \tag{26}$$

where a_{ls} and c_{ls} are the linear model constants.

Next, we consider the power consumption of the video source encoder of Section IV-B. Reference [13] proposes the following average power consumption model for an H.263 coder

$$P_s(\omega, R_s) = \frac{\epsilon_s f_r N_{\text{MB}}}{T} [(E_{\text{DCT}} + E_Q) + (T-1)(E_{\text{DCT}} + E_Q + E_{\text{ME}})] \tag{27}$$

where ϵ_s is the weighting factor introduced to allow for the scaling of the model based on the actual power consumption of a particular hardware and/or software implementation, f_r is

the frame rate, N_{MB} is the number of macroblocks in a frame, and T is described in Section IV-B. Further, E_{DCT}, E_Q, and E_{ME} respectively denote the energy consumed by DCT, quantization including the energy consumed by variable length coding (VLC), and motion estimation. Assuming

$$\begin{aligned} a_s &= f_r N_{\text{MB}} (E_{\text{DCT}} + E_{\text{ME}}) \\ b_s &= f_r N_{\text{MB}} E_{\text{ME}} \\ c_s &= f_r N_{\text{MB}} \frac{E_Q}{R_s} \end{aligned} \tag{28}$$

equation (27) can be expressed as

$$P_s(\omega, R_s) = \epsilon_s(a_s - b_s \omega + c_s R_s) \tag{29}$$

where a_s, b_s, and c_s are described in terms of the energy consumptions of different source coding components, ω is again the source coder INTRA rate, and R_s again indicates the source coding bit rate. The authors of [13] confirm that the measured power consumptions for encoding the sequences Containership.qcif, Foreman.qcif, MotherDaughter.qcif, News.qcif, and SilentVoice.qcif with an H.263 encoder fit the model parameters of (29) quite accurately. We note that the consistency of the models of (29) and (26) is verified by noting that when there is no motion estimation, i.e., all of the macro block are coded in INTRA-mode with $\omega = 1$, (29) is reduced to (26).

The second power consumption component of the underlying wireless system is the channel coder. Reference [4] models per bit energy consumption of a Reed–Solomon $RS(n, k)$ encoder as

$$P_c(R_s, R_c) = \epsilon_c \frac{n R_s R_c}{m(R_s + R_c)} \tag{30}$$

where ϵ_c is a scaling factor and m is the number of bits per symbol.

Finally, the third power consumption component of the underlying wireless system is the transmitter. The total transmission power is given by

$$P_t(R_s, R_c, E_{\text{sym}}) = \epsilon_t \frac{E_{\text{sym}}}{m}(R_s + R_c) \tag{31}$$

where ϵ_t is a scaling factor that maps the radiated energy into the actual transmission power of a wireless device. We note that the relative choice of the parameters ϵ_s, ϵ_c, and ϵ_t with respect to each other can identify whether the underlying coding techniques rely on hardware or software implementation. Using the existing technologies, ϵ_s is about two orders of magnitude greater than ϵ_c for both hardware and software implementations. However, ϵ_s and ϵ_t are of the same order of magnitude for a hardware implementation technique whereas the former is an order of magnitude larger than the latter for a software implementation technique [13]. While we focus on a hardware implementation technique in our work, investigating a software implementation technique is also straightforward.

Having expressed all of the power consumption components as well as the distortion terms, we now formulate our power

optimization problem subject to distortion and rate constraints as

$$\min_{\omega, R_s, R_c, E_{\text{sym}}} P_{\text{total}} = P_s + P_c + P_t \quad (32)$$

$$\text{Subject To}: \quad D_{\text{total}} = D_s + D_v \leq D_0 \quad (33)$$

$$R_{\text{total}} = R_s + R_c \leq R_0. \quad (34)$$

In the rest of this section, we use the general video source model of Section IV-B, making note of the fact that the model of (29) can be reduced to that of (26) by setting $\omega = 1$ and considering $a_{ls} = a_s - b_s$ and $c_{ls} = c_s$. We observe that for a single/multiple transmit/receive antenna wireless system utilizing the L-PSK modulation scheme, the objective function and inequality constraints of the above optimization problem can be expressed in terms of optimization variables ω, R_s, R_c, and E_{sym}, as well as some constants. The following equations illustrate the matter in the case of a double-transmit single-receive wireless system, the QPSK modulation scheme, the H.263 source encoder model of Section IV-B, and the Bernoulli channel. First, the total power is expressed as

$$P_{\text{total}} = \epsilon_s(a_s - b_s\omega + c_s R_s)$$
$$+ \epsilon_c \frac{nR_sR_c}{m(R_s + R_c)} + \epsilon_t \frac{E_{\text{sym}}}{m}(R_s + R_c). \quad (35)$$

Next, the distortion terms are expressed as

$$D_s = \frac{\theta_P + \Delta\theta_P \, \omega}{R_s - (R_{0P} + \Delta R_{0P} \, \omega)} + D_{0P} + \Delta D_{0P} \, \omega$$

$$D_v = \sigma_{u0}^2 \Psi \sum_{t=0}^{T-1} \frac{1 - \omega t}{1 + \lambda t}$$

$$= \sigma_{u0}^2 \sum_{t=0}^{T-1} \frac{1 - \omega t}{1 + \lambda t}$$

$$\sum_{k=t_c+1}^{n} \times \binom{n}{k} (e_{\text{sym}})^k (1 - e_{\text{sym}})^{n-k}. \quad (36)$$

Finally, the symbol error rate term is expressed as

$$e_{\text{sym}} = \frac{3}{4} - \frac{\zeta}{\pi} \left\{ \left(\frac{\pi}{2} + \tan^{-1}\zeta \right) \left(1 + \frac{2}{4 + E_{\text{sym}}} \right) \right.$$
$$\left. + \sin(2\tan^{-1}\zeta) \left(\frac{1}{4 + E_{\text{sym}}} \right) \right\} \quad (37)$$

where $\zeta = [E_{\text{sym}}/(4 + E_{\text{sym}})]^{1/2}$. The derivation of the equations is similar for the L-PSK modulation relying on (29), (30), (31) along with (22), (23), (2), (4), (9), and (24).

B. Power-Optimization Solutions

In this section, we provide a discussion of solving the optimization problem formulated by (32) along with the constraint set (33) and (34). Again considering the general form of (29), we use the video source model of Section IV-B in the discussion of this section. Further, we consider two scenarios.

In the first scenario, we assume that the cost function and the constraints of the optimization problem can all be expressed in closed form. Under the assumption of continuous differentiability, this results in introducing analytical solutions. Clearly, the case of the Bernoulli loss model and the Gilbert model are

covered under this scenario. Relying on the Lagrangian theory, we convert the problem to an optimization problem without constraints. We define the Lagrangian function of (32) as

$$LG_P = P_s + P_c + P_t + \mu_1(D_s + D_v - D_0) + \mu_2(R_s + R_c - R_0) \quad (38)$$

where the parameters μ_1 and μ_2 are the Lagrange multipliers in the Lagrangian Equation (38). The unconstrained minimization problem for $\Omega = \{\omega, R_s, R_c, E_{\text{sym}}\}$ is defined as

$$\min_{\Omega} LG_P = \min_{\Omega} \{P_s + P_c + P_t$$
$$+ \mu_1(D_s + D_v - D_0) + \mu_2(R_s + R_c - R_0)\}. \quad (39)$$

Conditions of Optimality: Constraint Qualifications: We now investigate the existence of necessary and sufficient optimality conditions also known as constraint qualifications. For our unconstrained minimization problem

$$\min_{\omega, R_s, R_c, E_{\text{sym}}} LG_P \quad (40)$$

the constraint qualifications are expressed in terms of Lagrange multiplier theory [2]. They revolve around conditions under which Lagrange multiplier vectors satisfying the following conditions are guaranteed to exist for a local minimum $\Omega^* = \{\omega^*, R_s^*, R_c^*, E_{\text{sym}}^*\}$. The local minimum satisfies

$$\nabla LG_P(\Omega^*) = 0 \quad (41)$$

where $\nabla LG_P = [(\partial LG_P/\partial\omega), (\partial LG_P/\partial R_s), (\partial LG_P/\partial R_c), (\partial LG_P/\partial E_{\text{sym}}), (\partial LG_P/\partial\mu_1), (\partial LG_P/\partial\mu_2)]$. Further, $\mu_k^* \geq 0$ for $k = 1, 2$ if associated with an active inequality at Ω^*, i.e.,

$$\begin{cases} \mu_1^* \geq 0, & \text{if } D_s + D_v = D_0 \\ \mu_1^* = 0, & \text{otherwise} \end{cases} \quad (42)$$

and

$$\begin{cases} \mu_2^* \geq 0, & \text{if } R_s + R_c = R_0 \\ \mu_2^* = 0, & \text{otherwise.} \end{cases} \quad (43)$$

Constraint qualifications guarantee the existence of unique Lagrange multipliers for a given local minimum Ω^* if the active inequality constraint gradients of (33) and (34) are linearly independent [2].

We note that the objective function (32) defined over a compact subset of $\mathcal{R}^4$ is continuously differentiable and the constraint gradients of (33) and (34) are linearly independent. Finding the solution to the optimization problem is, therefore, equivalent to finding the solution to the equation set (41) specifying optimization variables ω, R_s, R_c, and E_{sym}.

Further, it is important to observe that the formulated problem of (32) is subject to discrete constraints applied to the source coding variable $\omega = (1/T)$ and the channel coding variable $r = (k/n) = R_s/(R_s + R_c)$. Solving the problem of (32) is, hence, categorized under discrete constraint optimization problems which can be solved with the following approach. The approach is to add extra discrete constraints effectively changing the formulation of the optimization problem from a nonlinear programming (NLP) to a mixed integer nonlinear programming (MINLP) in which the variables ω and R_c can only take on discrete values. In this approach, one selects the best solution among the set of solutions to the problems obtained for different discrete values of the optimization parameters [2].

In the second scenario, we consider the cases in which the cost function and/or some of the optimization constraints cannot be expressed in closed form. This is clearly seen in the case of the Gilbert–Elliott loss model, in which the video coder distortion constraint of (24) cannot be expressed in a closed form. Considering the fact that constraints (33) and (34) are convex,[1] we propose deploying the sequential quadratic programming (SQP) technique. In SQP, the necessary conditions for optimality are represented by the Karush–Kuhn–Tucker (KKT) conditions described as the collection of (41) and the following relationships:

$$\mu_1^* (D_s^* + D_v^* - D_0^*) = 0$$
$$\mu_2^* (R_s^* + R_c^* - R_0^*) = 0$$
$$\mu_1^*, \mu_2^* \geq 0. \tag{44}$$

A variant of the quasi-Newton method can then be used to iteratively find the solution to the optimization problem [14]. This is equivalent to solving a quadratic estimation of the problem in every iteration.

We end this section by providing an analysis of the complexity for the two scenarios described above. Taking the discrete constraints into consideration and assuming p represents the number of parameter combinations, the time complexity of solving the problem of (41) for the first scenario is $\mathcal{O}(pd \log d)$, where d indicates the degree of (41). The complexity determines the overall complexity of the solution considering the fact that the rest of the calculations are in a lower time complexity order. Similarly, the time complexity of solving the problem of (41) for the second scenario is $\mathcal{O}(Ipd \log d)$ where I indicates the number of iterations and d indicates the degree of the quadratic estimation. We have observed that an average of ten and no more than twenty iterations are required for convergence in the case of the second scenario. The complexity results are, therefore, quite good compared to other recursive optimization approaches such as dynamic programming introducing a time complexity in the order of $\mathcal{O}(pd^2)$.

V. NUMERICAL ANALYSIS

In this section, we numerically validate our results. Before proceeding with the explanation of our numerical results, we note that we are solving the power optimization problem for both single and double-transmit antenna wireless systems. In the case of a double-transmit antenna system, we assume that two signals are transmitted simultaneously from the two transmit antennas at each time slot using STBCs of [1] and [19]. In addition, we assume that the slow fading wireless channel characterized by a Rayleigh distribution is quasistatic and flat implying that the path gains are constant over a frame but vary independently from one frame to another.

Our experiments simulate a wireless environment in which different uplink, downlink, and mobile-to-mobile transmission scenarios are possible. However considering the power limitation of mobile nodes, the scenarios of interest are uplink
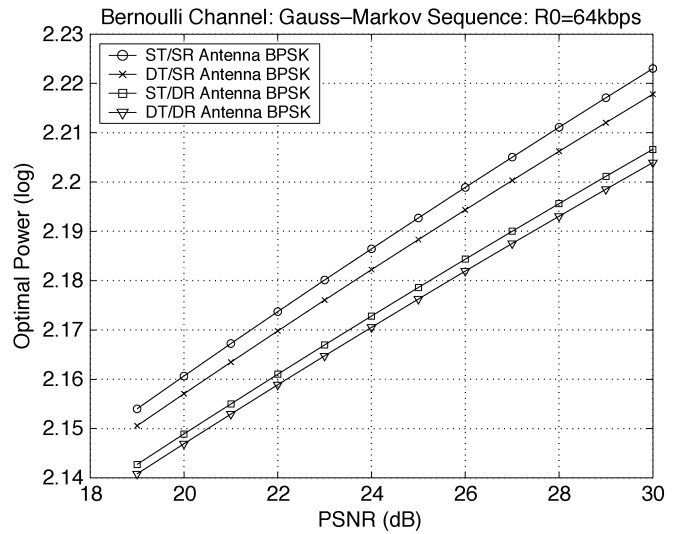

Fig. 3. BPSK plot of optimal power versus PSNR for single/double transmit/receive antenna systems. A Gauss–Markov source with parameter $\rho = 0.9$ and the Bernoulli loss model have been considered.
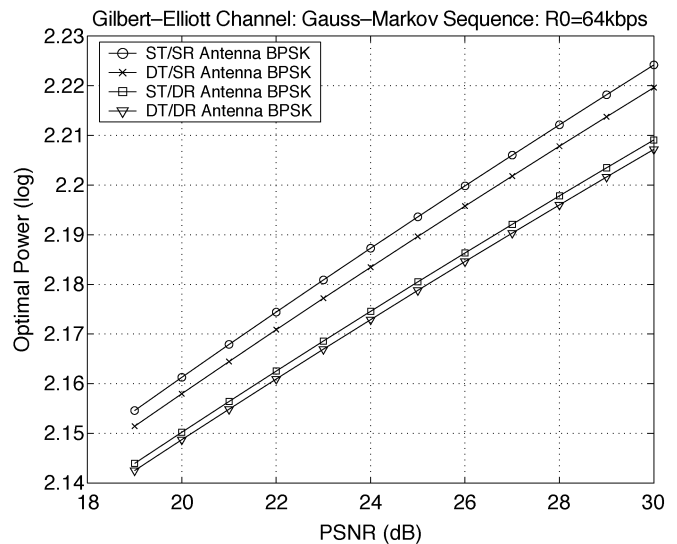

Fig. 4. BPSK plot of optimal power versus PSNR for single/double transmit/receive antenna systems. A Gauss–Markov source with parameter $\rho = 0.9$ and the Gilbert–Elliott loss model have been considered.

(mobile-to-base) and mobile-to-mobile transmissions. Assuming a mobile node may contain one or two transmit/receive antennas, we investigate different combinations of one or two transmit antennas with one or two receive antennas. More specifically, we consider four transmission scenarios: 1) a single-transmit single-receive (ST/SR) antenna system; 2) a single-transmit double-receive (ST/DR) antenna system; 3) a double-transmit single-receive (DT/SR) antenna system; and 4) a double-transmit double-receive (DT/DR) antenna system.

When utilizing the Gauss–Markov source of Section IV-A, we report our results for $\rho = 0.9$, indicating a highly correlated source with a behavior close to a video source and/or a speech source. Our experiments for the H.263 video source encoder of Section IV-B span over source coding parameter settings associated with the sequences Containership.qcif, Foreman.qcif,

---

[1]The function $f \colon \mathcal{C} \longmapsto \mathcal{R}^n$ defined over the convex set $\mathcal{C} \subseteq \mathcal{R}^n$ is called convex if $\forall x_1, x_2 \in \mathcal{C}$ and $0 \leq \alpha \leq 1$ the inequality $f(\alpha x_1 + (1 - \alpha)x_2) \leq \alpha f(x_1) + (1 - \alpha)f(x_2)$ holds.

MotherDaughter.qcif, News.qcif, and SilentVoice.qcif. However, we only report the results for Containership.qcif and Foreman.qcif. In addition, we select the scaling factors $[\epsilon_s, \epsilon_c, \epsilon_t]$ as $[1, 0.01, 1]$ representing transmission systems using hardware coding implementation.

Despite the fact that our experimentation set up is fairly close to that of [13], we do not directly compare our results of utilizing the video source encoder of Section IV-B with the results reported there. This is because our model relies on the more general Gilbert–Elliott model rather than the Gilbert model of [16] and [13]. Furthermore, our model relates the average received signal-to-noise ratio to a Rayleigh distribution rather than the distance. We believe that our model is more suitable for wireless channels due to the considerations of the fading effects. Instead, we compare the results of utilizing ST/SR, DT/SR, ST/DR, and DT/DR antenna systems in a Rayleigh fading channel under both Bernoulli and Gilbert–Elliot loss models. We also note that when the loss behavior of the channel is characterized by the Gilbert–Elliott model, we set $\mathcal{E}[|\alpha_G|^2] = 10\mathcal{E}[|\alpha_B|^2]$ to distinguish between the GOOD state and the BAD state. In the latter case, the parameters of the model $[\gamma, \beta]$ are set to $[0.998\,73, 0.875]$ indicating an average burst length $L_B = 1/(1 - \beta) = 8$. Setting a block length of $n = 222$ symbols for the RS coder with BPSK and QPSK modulations, we allow the H.263 video source coding variable T and channel coding variable k to assume values from the discrete sets $[2, 3, 5, 9, 12, 16, 25, 32]$ and $[40, 50, 60, 70, 80, 90, 100, 112, 122, 132, 142, 152, 162, 172, 182, 192, 202]$, respectively. For a given bit rate R_0 of up to 256 kbps, indicating the achievable bit rate of the 3G wireless standard, we plot the optimal power values obtained for maximum acceptable distortion measures. We map the distortion measure D_0 to peak signal-to-noise ratio (PSNR) measure as PSNR $= 10log_{10}(255^2/D_0)$ when comparing different combinations of transmit and receive antennas together.

Utilizing the Gauss–Markov source of Section IV-A, Fig. 3 plots the optimal values of P_{total}, the total power for the BPSK modulation scheme versus the PSNR. We note that the PSNR metric is used instead of the more meaningful distortion metric in order to provide consistency with the plots of the video sequences provided next. The results have been obtained for normalized values of ξ, σ_{gm}^2, $\mathcal{E}[|\alpha|^2]$, N_0, and a channel loss characterized by the Bernoulli model. Fig. 4 plots similar curves for normalized values of ξ, σ_{gm}^2, $\mathcal{E}[|\alpha_G|^2]$, N_0, and a channel loss characterized by the Gilbert–Elliott model.

The most striking observation when comparing the results of the figures is the fact that the optimal power of a DT/DR antenna system is consistently lower than that of the rest. In addition, the optimal power of an ST/SR antenna system is higher than that of the rest. Comparing the optimal power of an ST/DR antenna system with that of a DT/SR antenna system, we observe that the former introduces a lower optimal power. Considering the fact that the diversity gain is in the order of the product of the transmit and the receive antennas, both schemes achieve a diversity gain of order two. However, recalling the discussion of Section III-A, we note that from the signal-to-noise ratio standpoint, the power efficiency of the latter scheme suffers a 3-dB loss
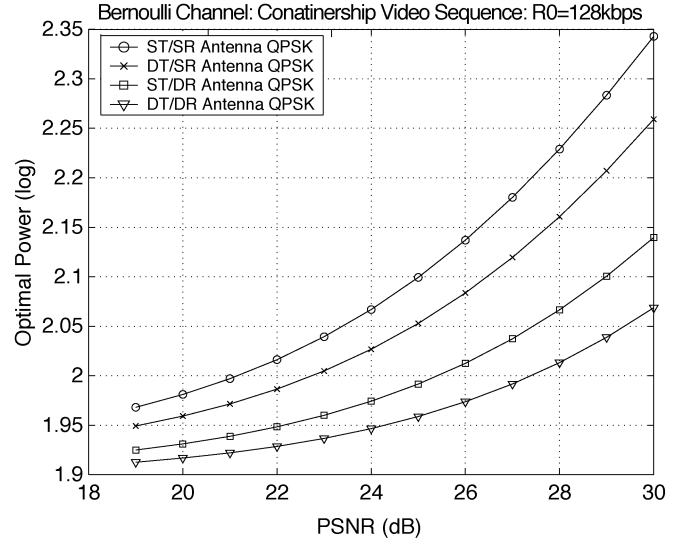

Fig. 5. QPSK plot of optimal power versus PSNR for single/double transmit/receive antenna systems. Containership.qcif video source and the Bernoulli loss model have been considered.
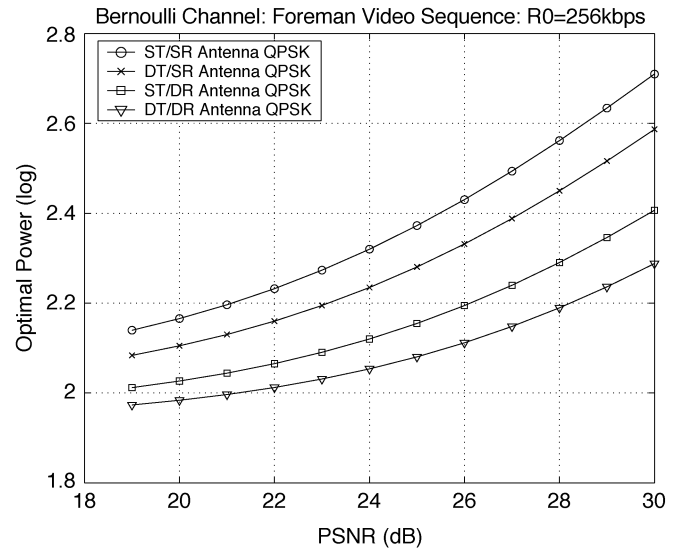

Fig. 6. QPSK plot of optimal power versus PSNR for single/double transmit/receive antenna systems. Foreman.qcif video source and the Bernoulli loss model have been considered.

compared to that of the former scheme for the same transmission power. This justifies the lower optimal power of an ST/DR antenna system compared to that of a DT/SR antenna system.

In addition, the following comments are in order. First, we observe that plotting the optimal values of power P_{total} versus the values of available bit rate R_0 for a fixed quality of service PSNR or D_0 yields similar qualitative results as the ones shown in the above figures, i.e., the optimal power curves are nondecreasing functions of the available bit rates R_0. However, we have observed that the impact of increasing the value of R_0 for a given PSNR on the overall optimal power is not as significant as the impact of increasing the value of PSNR for a given R_0. In other words, the four curves illustrated in different figures are closer to each other. Second, comparing the results of Containership.qcif with those of Foreman.qcif, we observe similar
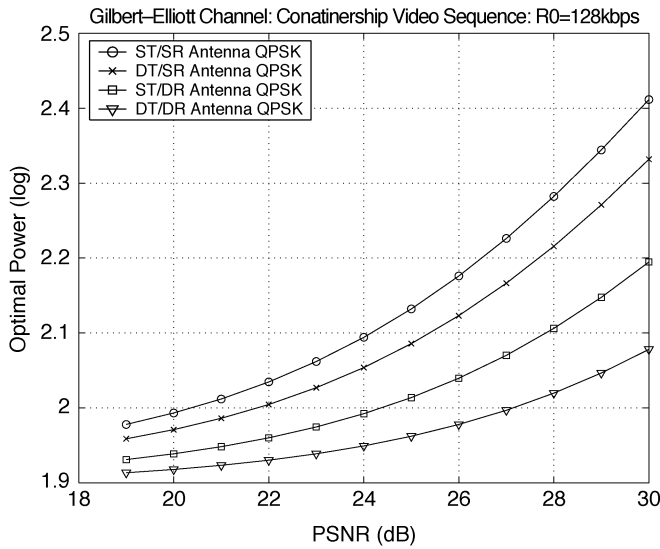
Fig. 7. QPSK plot of optimal power versus PSNR for single/double transmit/receive antenna systems. Containership.qcif video source and the Gilbert–Elliott loss model have been considered.

Fig. 9. Total optimal power and its allocation among source coding, channel coding, and transmission. An ST/SR antenna system, QPSK modulation, Foreman.qcif video source, and the Bernoulli loss model have been considered.

Utilizing the Containership and Foreman video sequences, Figs. 5 and 6 respectively plot the optimal values of the total power for the QPSK modulation scheme versus the PSNR. The results have been obtained for normalized values of σ_{u0}^2, $((2\mathcal{E}[|\alpha|^2])/N_0)$, and a channel loss characterized by the Bernoulli model. Fig. 7 and Fig. 8 plot similar curves for normalized values of ξ, σ_{gm}^2, $((2\mathcal{E}[|\alpha|^2])/N_0)$, and a channel loss characterized by the Gilbert–Elliott model.

At the end of this section, we study the distribution of the power components. Fig. 9 shows a sample plot of the optimal power components of source coding P_s, channel coding P_c, and transmission P_t along with the total optimal power P_{total} for an ST/SR antenna system. We provide a set of observations that are based on Fig. 9 and similar figures not shown here for DT/SR, ST/DR, and DT/DR antenna systems. The first important observation is that the allocation of power is qualitatively the same for different choices of video sources, channel models, and number of transmit/receive antennas. The allocation of source coding power increases very little while the allocation of channel coding and transmission powers increase with much higher rates for higher QoS metrics. We have also observed that the distance between the curves of P_t and P_c remain the same for different choices of system parameters. The second observation is that by increasing the number of transmit and/or receive antennas the intersection point of the plots of transmission and source coding shifts to the right. This indicates that less power has to be assigned to the transmission component as the result of improving transmission efficiency. The intersection point moves from the left to the right for the combinations ST/SR, DT/SR, ST/DR, and DT/DR antenna systems.
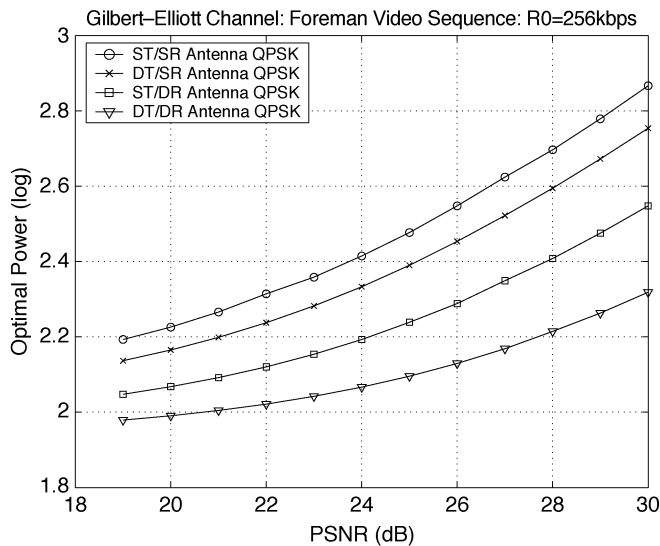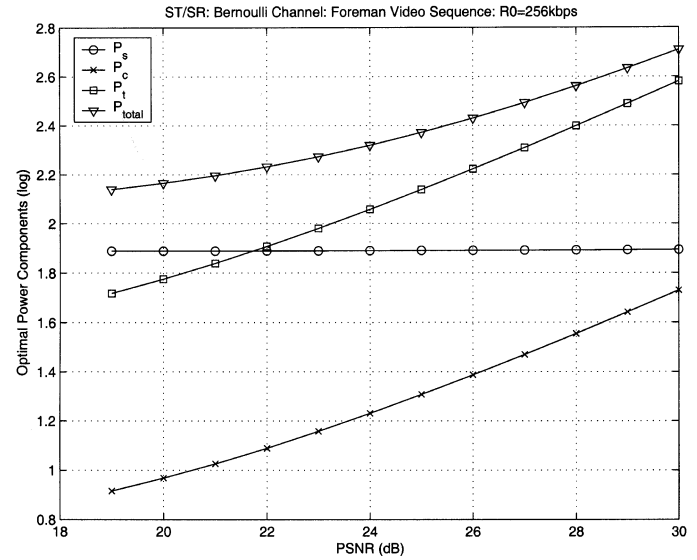

Fig. 8. QPSK plot of optimal power versus PSNR for single/double transmit/receive antenna systems. Foreman.qcif video source and the Gilbert–Elliott loss model have been considered.

qualitative behaviors with higher optimal power values in the case of the second sequence. The results are expected considering the higher motion of the second sequence compared to the first. Third, we have conducted another set of experiments for a channel loss characterized by the Gilbert–Elliott model and an average burst length of $L_B = 1/(1 - \beta) = 32$. Although not shown in the figures, our findings exhibit a similar qualitative behavior and are consistent with the reported results of this section. Fourth, we observe a similar qualitative behavior regardless of utilizing BPSK or QPSK. Finally, we note that the choice of scaling factors in our reported experiments indicates a scenario in which source and channel coders are implemented in hardware. The results of software implementation are similar and are not reported here.

VI. CONCLUSION

In this paper, we presented some solutions to the general problem of power control in wireless media systems with multiple antennas. We provided an analysis of the underlying

wireless system consisting of transmitting, channel, and receiving sides. Relying on our analysis results, we formulated an optimization problem aimed at minimizing the total power consumption of wireless media systems subject to a given quality of service level and an available bit rate. Our formulation considered the power consumption related to source coding, channel coding, and transmission of double-transmit antennas. While our source coding analysis used both a Gauss–Markov source and a video source, our channel coding analysis relied on a Rayleigh fading channel along with the Bernoulli/Gilbert–Elliott loss models. Finally, our transmission analysis used space-time block codes. We evaluated the performance of our power optimized solution for both single/double transmit/receive antenna systems and observed that utilizing a double-transmit double-receive antenna system provided the lowest optimal power values. The optimal power values of a single-transmit double-receive antenna system were the next best followed by those of a double-transmit single-receive antenna system and a single-transmit single-receive antenna system.

We are currently working on the expansion of our results into the layered and replicated media scenarios as a general combined framework for distributing multimedia content over the wireless backbone. We are focusing on both coding and networking aspects of the problem. In addition, we are developing novel content processing algorithms capable of providing video summaries, thereby further reducing the power consumption of a wireless system.

REFERENCES

[1] S. M. Alamouti, "A simple transmitter diversity scheme for wireless communications," *IEEE J. Select. Areas Commun.*, vol. 16, pp. 1451–1458, Nov. 1998.

[2] D. P. Bertsekas, *Nonlinear Programming*, 2nd ed. Belmont, MA: Athena, 1999.

[3] E. O. Elliott, "Estimates on error rates for codes on burst-noise channels," *Bell Syst. Tech. J.*, vol. 42, Sept. 1963.

[4] S. Appadwedula, M. Goel, N. R. Shanbhad, D. L. Jones, and K. Ramchandran, "Total system energy minimization for wireless image transmission," *J. VLSI Signal Processing Syst.*, vol. 27, no. 1/2, Feb. 2001.

[5] A. Gersho and R. M. Gray, *Vector Quantization and Signal Compression*. Norwell, MA: Kluwer, 1992.

[6] E. N. Gilbert, "Capacity of a burst-noise channel," *Bell Syst. Tech J.*, vol. 39, Sept. 1960.

[7] M. Goel, S. Appadwedula, N. R. Shanbhag, K. Ramchandran, and D. L. Jones, "A low-power multimedia communication system for indoor wireless applications," in *Proc. IEEE Workshop on SIPS*, Oct. 1999, pp. 478–482.

[8] P. J. M. Havinga, "Energy efficiency of error correction on wireless systems," in *Proc. IEEE WCNC*, Sept. 1999.

[9] H. Jafarkhani, P. Ligdas, and N. Farvardin, "Adaptive rate allocation in a joint source-channel coding framework for wireless channels," in *Proc. IEEE VTC*, vol. 1, May 1996, pp. 492–496.

[10] H. Jafarkhani, H. Yousefi'zadeh, and M. Moshfeghi, "Power optimization of memoryless wireless media systems with space-time block codes," in *Proc. IEEE GLOBECOM*, vol. 1, Dec. 2003, pp. 123–127.

[11] Z. Ji, Q. Zhang, W. Zhu, and Y.-Q. Zhang, "End-to-end power-optimized video communication over wireless channels," in *Proc. IEEE Workshop MMSP*, Oct. 2001, pp. 447–452.

[12] T. H. Lan and A. H. Tewfik, "Adaptive low power multimedia wireless communications," in *Proc. IEEE Workshop on MMSP*, June 1997, pp. 377–382.

[13] X. Lu, Y. Wang, and E. Erkip, "Power efficient H.263 video transmission over wireless channels," in *Proc. IEEE ICIP*, vol. 1, Sept. 2002, pp. 533–536.

[14] D. F. Shanno, "Conditioning of quasinewton methods for function minimization," *Mathem. Comput.*, vol. 24, 1970.

[15] M. K. Simon and M. S. Alouini, *Digital Communication Over Fading Channels: A Unified Approach to Performance Analysis*. New York: Wiley, 2000.

[16] K. Stuhlmuller, N. Farber, M. Link, and B. Girod, "Analysis of video transmission over lossy channels," *IEEE J. Select. Areas Commun.*, vol. 18, pp. 1012–1032, June 2000.

[17] C. C. Tan and N. C. Beaulieu, "On first-order Markov modeling for the Rayleigh fading channel," *IEEE Trans. Commun.*, vol. 48, pp. 2032–2040, Dec. 2000.

[18] V. Tarokh, H. Jafarkhani, and A. R. Calderbank, "Space-time block coding for wireless communications: performance results," *IEEE J. Select. Areas Commun.*, vol. 17, pp. 451–460, Mar. 1999.

[19] ——, "Space-time block coding from orthogonal designs," *IEEE Trans. Inform. Theory*, vol. 45, pp. 1456–1467, July 1999.

[20] H. Yousefi'zadeh and H. Jafarkhani, "Statistical guarantee of QoS in communication networks with temporally correlated loss," in *Proc. IEEE GLOBECOM*, Dec. 2003, pp. 4039–4093.

Homayoun Yousefi'zadeh (S'96–M'98) received the B.S. degree from Sharif University of Technology, Tehran, Iran, the M.S. degree from Amirkabir University (Tehran Polytechnic Institute), Tehran, and the Ph.D. degree from the University of Southern California, Los Angeles, all in electrical engineering, in 1989, 1993, and 1997, respectively.

He is currently an Assistant Adjunct Professor in the Department of Electrical Engineering and Computer Science, University of California, Irvine. Most recently, he was the CTO of TierFleet, Inc., working on distributed database systems, a Senior Technical and Business Manager at Procom Technology, focusing on storage networking, and a Technical Consultant at NEC Electronics, designing and implementing distributed client–server systems. He is the inventor of three patents.

Dr. Yousefi'zadeh has been with the technical program committees of various IEEE and ACM conferences. He has also served as the Chairperson of systems' management workgroup of the Storage Networking Industry Association (SNIA), as a member of the Scientific Advisory Board of Integrated Media Services Center (IMSC) at the University of Southern of California, and as a member of American Management Association.

Hamid Jafarkhani (S'93–M'97–SM'01) received the B.S. degree in electronics from Tehran University, Tehran, Iran, in 1989 and the M.S. and Ph.D. degrees, both in electrical engineering, from the University of Maryland at College Park in 1994 and 1997, respectively.

From June 1996 to September 1996, he was a summer intern at Lucent Technologies (Bell Labs). He joined AT&T Labs–Research as a Senior Technical Staff Member in August 1997. Later, he was promoted to a Principle Technical Staff Member. He was with Broadcom Corporation as a Senior Staff Scientist from July 2000 to September 2001. Currently, he is an Associate Professor in the Department of Electrical Engineering and Computer Science, University of California, Irvine, where he is also the Deputy Director of the Center for Pervasive Communications and Computing.

Dr. Jafarkhani is an Associate Editor for the IEEE COMMUNICATIONS LETTERS and the IEEE TRANSACTIONS ON WIRELESS COMMUNICATIONS. He was a co-recipient of the American Division Award of the 1995 Texas Instruments DSP Solutions Challenge, and received the Best Paper Award of ISWC in 2002 and a National Science Foundation Career Award. In 1984, he ranked first in the nationwide entrance examination of Iranian universities.

Mehran Moshfeghi received the B.S. degree (first-class honors) in physics and mathematics and the Ph.D. degree in physics in 1982 and 1985, respectively, both from the University of Bristol, Bristol, U.K.

From 1985 to 1999, he was a Senior Member of Technical Staff at Philips Research Laboratories, where he worked on image reconstruction, image processing and analysis algorithms, distributed medical information systems, and Internet computing. He was with Zaplet Inc. as a Senior Architect from 1999 to 2000, where he developed collaboration software systems. Currently, he is an Associate Adjunct Professor in the Department of Electrical Engineering and Computer Science, University of California, Irvine. He has six patents issued.

Dr. Moshfeghi obtained the Albert Fry Prize in 1982, awarded to the best student graduating in the Faculty of Science of Bristol University. He was a recipient of a University of Bristol Scholarship and Royal Society's Paul Instrument Fund from 1982 to 1985. He received four Philips Research Merit achievement awards.